



Contents lists available at ScienceDirect

Journal of Biomechanics

journal homepage: www.elsevier.com/locate/jbiomech
www.JBiomech.com

The response of the pediatric head to impacts onto a rigid surface

Andre Matthew Loyd^{*}, Roger W. Nightingale, Jason F. Luck, Cameron 'Dale' Bass, Hattie C. Cutcliffe, Barry S. Myers

Duke University Injury Biomechanics Laboratory, United States

ARTICLE INFO

Article history:

Accepted 29 June 2019

Available online xxxx

Keywords:

Head
Pediatric
Impact
Injury
Biomechanics
Acceleration
Head Injury Criterion (HIC)
Stiffness
Impulse
Fracture

ABSTRACT

The study of pediatric head injury relies heavily on the use of finite element models and child anthropomorphic test devices (ATDs). However, these tools, in the context of pediatric head injury, have yet to be validated due to a paucity of pediatric head response data. The goal of this study is to investigate the response and injury tolerance of the pediatric head to impact.

Twelve pediatric heads were impacted in a series of drop tests. The heads were dropped onto five impact locations (forehead, occiput, vertex and right and left parietal) from drop heights of 15 and 30 cm. The head could freely fall without rotation onto a flat 19 mm thick platen. The impact force was measured using a 3-axis piezoelectric load cell attached to the platen.

Age and drop height were found to be significant factors in the impact response of the pediatric head. The head acceleration (14–15 cm; 103–30 cm), Head Injury Criterion (HIC) (253–15 cm; 154–30 cm) and impact stiffness (5800–15 cm; 3755–30 cm) when averaged across all impact locations increased with age from 33 weeks gestation to 16 years, while the pulse duration (66–15 cm; 53–30 cm) decreased with age. Increases in head acceleration, HIC and impact stiffness were also observed with increased drop height, while pulse duration decreased with increased drop height.

One important observation was that three of the four cadaveric heads between the ages of 5-months and 22-months sustained fractures from the 15 cm and 30 cm drop heights. The 5-month-old sustained a right parietal linear fracture while the 11- and 22-month-old sustained diastatic linear fractures.

© 2019 Published by Elsevier Ltd.

1. Introduction

Child head injury takes a substantial human toll with large numbers of deaths, permanent disability and costly treatments. There are approximately 700,000 head injuries for children 19-years-old and younger annually in the United States, resulting in more than 6000 deaths. Children between the ages of 0–4 and 15–19 are the two most likely groups to sustain a head injury with the majority of these head injuries occurring due to falls or motor vehicle crashes (Faul et al., 2010). In addition to mortality, head injuries cause visual and balance problems as well as cognitive problems such as memory loss and concentration lapses (Ilie et al., 2014; McKinlay et al., 2008).

Unlike the adult head, much of the available literature on the biomechanics of pediatric head injury is limited due to a lack of pediatric specimens (Prange et al., 2004). As a result, researchers have relied on finite element (FE) analyses and anthropomorphic testing devices (ATDs) to investigate the biomechanics of the pedi-

atric head in impact. Current pediatric injury risk curves were developed using these tools, but they depend heavily on scaling from adult head properties to the pediatric head (Coats et al., 2007; Klinich et al., 2002; Van-Ee et al., 2009). However, these scaling rules, ATDs and FE models have not been validated or benchmarked against pediatric data (Melvin, 1995; Mertz et al., 2001; Van-Ee et al., 2009; van-Ratingen et al., 1997).

As a result, even fundamental issues in pediatric injury biomechanics remain uncertain. For example, there is currently disagreement in the literature over the risk of pediatric skull fracture from minor falls (Billmire and Myers, 1985; Hobbs, 1984; Leventhal et al., 1993). One consequence of this uncertainty is that there are no criteria for which injuries are associated with physical abuse and which injuries are associated with accidental falls. Because the human skull continues to develop into adulthood, with changing structural and material properties, the results of adult skull fracture studies have limited application to pediatric head injury (Coats and Margulies, 2006; Currey and Butler, 1975; Gurdjian et al., 1950; Hodgson and Thomas, 1971b; Manzanares and Goret-Nicaise, 1988; Margulies and Thibault, 2000). Weber conducted a series of cadaveric tests using 50 post-mortem human

^{*} Corresponding author.

E-mail address: andre.m.loyd@gmail.com (A.M. Loyd).

infant skulls less than 9-months-old and analyzed skull fractures from impact heights of 820 mm onto five different types of surfaces: stone, carpet, foam, camel hair blanket and linoleum (Weber, 1984, 1985). These studies provide insight into fracture risk, but did not record the impact response of any of the heads. Hence, the goals of this study are (1) to evaluate the impact response of a sample of pediatric heads ranging in age from 33-weeks-gestation to 16-years-old onto a rigid surface, (2) measure the response of the pediatric head to benchmark current pediatric head injury tools and scaling rules and (3) to assess the pediatric skull's risk of fracture.

2. Methods

The same twelve pediatric heads from Loyd et al., 2015 were used for this study (Table 1). These head impact tests were performed following a cervical spine testing series and before head compression tests (Loyd et al., 2015; Luck et al., 2008; Luck et al., 2013a; Luck et al. 2013b). The heads were disarticulated from the cervical spine at the occipital condyles in the atlanto-occipital joint. The mandibles of all specimens had been removed for the prior cervical spine testing. The head anthropometries are reported in Table 1. Left and right external auditory meatuses (EAMs), infraorbital foramen (IOF) and the Frankfort plane were marked (Walker et al., 1973). Each head was filled with saline (0.9% NaCl solution) to remove all air voids and the foramen magnum was sealed across the occipital condyles with poly(methyl methacrylate) (PMMA). The resulting mass of the head was recorded.

The drop tests were performed using two drop heights, 15 cm followed by 30 cm, onto five impact locations. The 15 cm drops were conducted first and the impact locations were tested in the following order: forehead, occiput, vertex, right parietal and left parietal. The drop heights were selected to minimize the risk that fractures would occur during the impacts and to make the test "non-destructive" (Hodgson and Thomas, 1971b; Prange et al., 2004). After each head drop, the head was palpated for fractures and the force-time plots were checked for evidence of fractures.

For each drop, the head was placed into a finely meshed net that was attached to a pulley using nylon line. The head was positioned inside the net to set the desired impact location. The head was then adjusted to the desired drop height and released by burning the nylon line to ensure free fall without rotation. The head impacted a smooth, flat aluminum platen that was 3/4-inches thick and was

attached to a Kistler 3-axis piezoelectric load cell (Kistler, France). Force-time data were recorded using LabVIEW (National Instruments, Austin, TX) at a sample rate of 100,000 Hz. All head drops were recorded using a Phantom high-speed digital video camera (Vision Research, Inc., Wayne, NJ). Approximately, five minutes passed between subsequent drops.

The force data was filtered using the SAE J211b Class 1000 standard (SAEJ222-1, 1995). The average linear acceleration of the head was estimated by dividing the force history by the specimen head mass. Using this estimate and the pulse duration, the peak resultant acceleration, head injury criterion (HIC) and impact stiffness were calculated (Kleinberger et al., 1998) (Eq. (1)). Force-displacement curves were estimated by integrating the acceleration-time histories and taking the force from the load cell. The displacement was calculated by double integrating the estimated acceleration-time pulse. To calculate impact stiffness, the force-displacement curve was regressed from 50% of the peak displacement to peak force. Hence, using the linear region of the force-displacement curve to calculate the impact stiffness. The duration of the impulse was calculated by the time points at which the force-time pulse crossed 0.1% of the full range of the force.

$$HIC = \max_{t_1, t_2} \left\{ \left[\frac{1}{t_2 - t_1} \int_{t_1}^{t_2} a(t) dt \right]^{2.5} (t_2 - t_1) \right\} \quad (1)$$

Statistical analysis was performed using SAS v 9.3 (SAS Institute, Cary, NC) with a significance level of $p < 0.05$. Linear mixed models (PROC MIXED), with the specimen as a random effect, were used to account for the repeated testing. Each specimen generally underwent ten impact tests (two heights and five locations). The independent variables were age, drop height and impact location. The measured responses were peak force, impulse duration, and hysteresis. The calculated responses were peak acceleration, HIC, and stiffness. Pearson correlation coefficients of this same sample from Loyd et al., 2015 showed that all the anthropometric variables were highly correlated with age. Therefore, they were not included as predictors in the regression models since they were represented by age. Backwards selection was used to determine the most parsimonious model, in which all independent variables were included in the initial fitted model. Then, any independent variables that had a non-significant contribution to the model were removed from the analysis, and the simplified model was re-fit to the data. This parsimonious model, including only the statistically significant independent variables, was reported as the final model describing the data.

Table 1
Pediatric heads used in head impact tests.

Specimen ID	Age	Age (m)	Sex	Drop Mass (kg)	Race	Head Length (cm)	Head Width (cm)	Head Circ. (cm)	Age Group	Cause of death
P13F	34-week-gest.	-1.35	F	0.448	Unknown	10.7	7.2	29.7	Neonate	Unknown
P07M	33-week-gest.	-1.575	F	0.417	Unknown	9.9	8.4	29.6	Neonate	Unknown
P08M	37.5-week-gest.	-0.5625	M	0.6467	Caucasian	12.6	9.6	35.8	Neonate	Pulmonary Hypoplasia
P05F	1-day-old	0.03	F	0.6011	Caucasian	10.8	9	33.4	Neonate	Diaphragmatic hernia
P03M	3-day-old	0.1	M	0.4153	Caucasian	10.3	8.5	30.4	Neonate	Ischemic encephalopathy; cerebral infarction
P06F	11-day-old	0.36	F	0.6467	Black	10.8	9.5	34.8	Neonate	Non-immune hydrops fetalis; intercranial hemorrhage
P12M	5-month-old	5	M	1.071	Black	13.1	10.9	40.8	Infant	Respiratory failure
P14M	9-month-old	9	M	1.76	Black	14.8	12	46.5	Infant	Chronic obstructive pulmonary Disease
P15F	11-month-old	11	F	1.45	Caucasian	14.8	12.2	44.5	Infant	SIDS, renal failure
P17F	22-month-old	22	F	2.05	Caucasian				Infant	Non-Hodgkins lymphoma
P18M	9-years-old	108	M	2.17	Black	16.9	13	49.3	Youth	End stage renal disease; secondary: Hyperkalemia
P21F	16-years-old	192	F	3.07	Caucasian	19.2	14.5	56.6	Youth	Seizure disorder

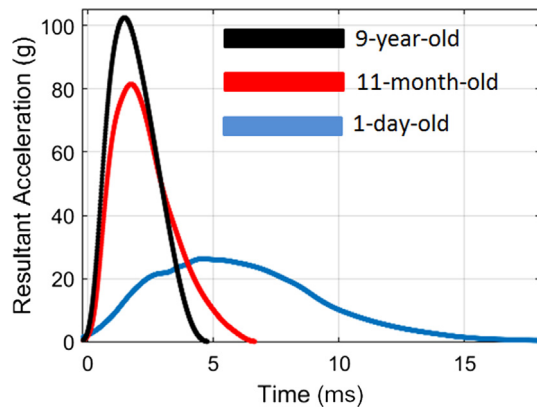


Fig. 1. Typical forehead 15 cm impact response for three different ages. Pulse duration decreased with age and peak acceleration increased with age.

3. Results

Examples of the impact responses are shown in Figs. 1 through 3, while Table 2 presents all of the impact response data. In general, the younger specimens were more compliant than the older specimens with lower peak forces and longer impulse durations (Figs. 4 and 5).

The final fit parameters for all the dependent variables are shown in Table 3. The linear mixed model showed that the peak force was dependent on age ($p < 0.0001$) and drop height ($p < 0.0001$). The impact location was not significant ($p = 0.08$); however, the occipital impacts generated qualitatively large forces (Fig. 4). The impulse duration was dependent on age ($p < 0.0001$) and drop height ($p = 0.0003$). Although the individual impact loca-

tions had p -values greater than 0.05 for impulse duration, the overall effect of location in the fixed effect test was also significant ($p = 0.006$). The energy dissipated was also dependent on age ($p < 0.03$), location ($p < 0.0001$), and height ($p = 0.03$) Fig. 6.

For the calculated responses, the peak acceleration was predicted by age ($p < 0.0001$), drop height ($p < 0.0001$), and location ($p = 0.02$). For the HIC, the significant predictors were age ($p = 0.0001$) and height ($p < 0.0001$) but not location ($p = 0.10$). For the impact stiffness, the only significant predictor was age. Neither height ($p = 0.6$) nor location ($p = 0.09$) were significant, which may be due to the limited number of samples.

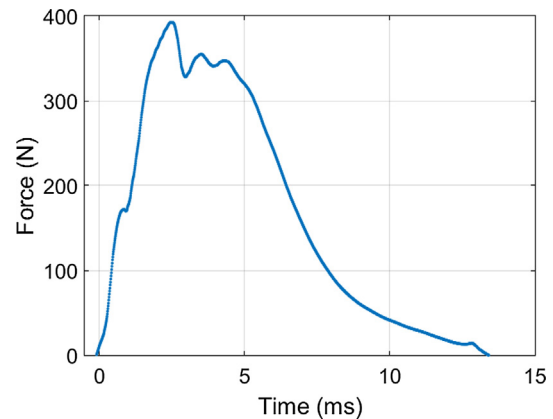


Fig. 3. Force-time curve for the 15 cm parietal drop from the 5-month-old (P12M). The documented linear fracture to the right parietal bone occurred on this 15 cm drop as shown by the force plateau and the extended pulse duration tail (Hodgson and Thomas, 1971a; 1971b).

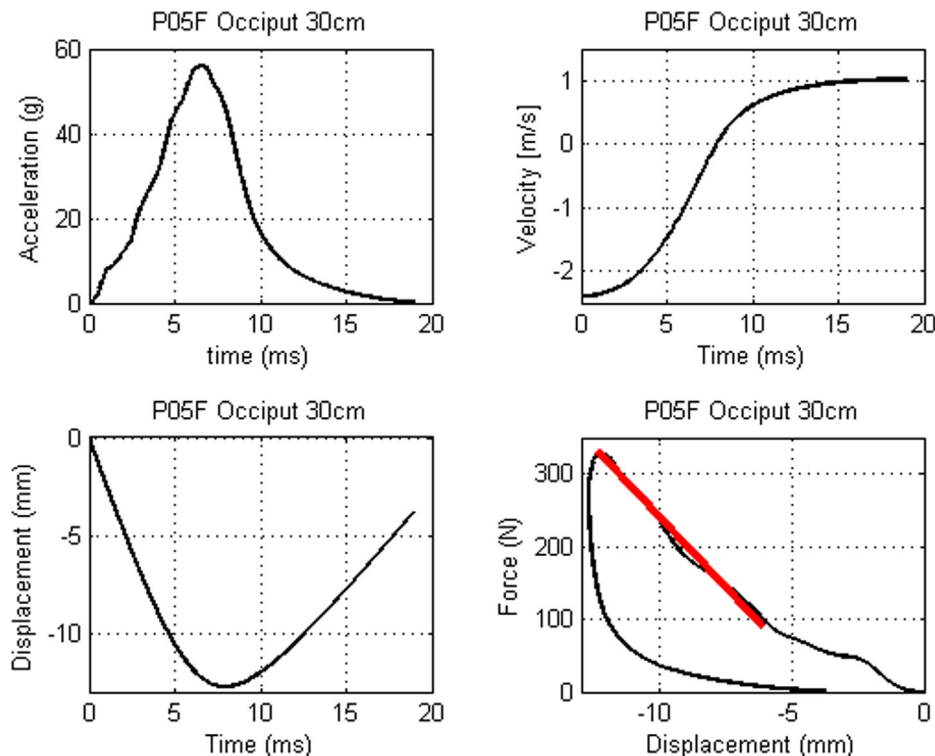


Fig. 2. Example plots of the acceleration, velocity and displacement during impact for a neonatal 30 cm occipital head drop (P05F). The acceleration is shown on the top left. The velocity is shown on the top right and was calculated by integrating the acceleration. The displacement is shown on the lower left and was calculated by integrating the acceleration. The stiffness was calculated from the force-displacement plot from the peak force to 50% of displacement and is noted by the red line in the bottom right plot. (For interpretation of the references to colour in this figure legend, the reader is referred to the web version of this article.)

Table 2
Impact data for the pediatric head drops. * denotes that data is post fracture for P12M.

Specimen	Drop Location	Force (N)		Acceleration (g)		HIC		Impact Stiffness (N/mm)		Pulse Duration (ms)		Hysteresis Lost (%)	
		15 cm	30 cm	15 cm	30 cm	15 cm	30 cm	15 cm	30 cm	15 cm	30 cm	15 cm	30 cm
P03M	Vertex	264	461	64.5	112.4	64	204	49	83	13.7	11.7	59	63
P03M	Occiput	189	296	46	72.1	48	109	30	35	12.9	12.8	57	66
P03M	Forehead	205	334	49.5	82.1	55	178	44	37	12.9	12	63	62
P03M	Right Parietal	194	317	48	77.6	49	137	34	56	12.8	12.9	67	70
P03M	Left Parietal	170	253	41	61.9	39	112	24	21	13	12.3	75	71
P05F	Vertex	220	337	37.3	57.1	29	71	33	42	26	22.1	77	87
P05F	Occiput	209	330	35.4	55.9	24	71	30	39	22.5	18.8	73	82
P05F	Forehead	154	225	26.1	38	17	38	18	21	22.6	22.1	95	99
P05F	Right Parietal	190	326	32.2	55.2	24	70	14	33	25	18.5	90	91
P05F	Left Parietal	220	311	37.2	52.6	27	71	28	35	19.1	17.4	87	89
P06M	Vertex	262	473	41.3	74.6	28	96	31	50	23.9	20.1	74	77
P06M	Occiput	208	336	32.7	52.9	25	75	26	39	23.5	20.6	71	74
P06M	Forehead	167	273	26.3	43.1	20	47	12	15	23.4	20.7	77	85
P06M	Right Parietal	212	305	33.4	48	22	59	24	26	20.1	17	85	83
P06M	Left Parietal	204	292	32.1	46.1	22	64	25	21	20.8	18	81	84
P07M	Vertex	180	339	43.9	83	36	136	28	54	17.22	14.64	82	80
P07M	Occiput	174	216	42.6	52.7	29	66	27	21	14.79	14.69	89	88
P07M	Forehead	216	354	52.7	86.6	55	172	51	80	11.65	10.57	85	83
P07M	Right Parietal	171	301	41.8	73.5	34	113	28	43	14.47	12.38	89	89
P07M	Left Parietal	156	323	38	78.9	28	115	17	51	18.92	12.4	90	89
P08M	Vertex	241	336	36.4	50.7	26	57	33	30	22.43	22.06	83	90
P08M	Occiput	170	287	25.6	43.3	16	43	17	24	23.53	21.89	81	85
P08M	Forehead	192	285	28.9	43	18	51	21	16	23.53	21.1	86	93
P08M	Right Parietal	189	320	28.5	48.2	17	43	25	137	23.45	17.54	93	93
P08M	Left Parietal	160	362	24.2	54.6	14	68	12	45	22.7	19.9	93	92
P12M	Vertex	472	753	44.9	71.6*	42	118*	93	125*	14.23	13.28*	78	80*
P12M	Occiput	459	851	43.7	81*	42	132*	91	159*	14.44	12.27*	72	81*
P12M	Forehead	468	605	44.5	57.6*	42	82*	83	61*	13.29	13.92*	82	88*
P12M	Right Parietal	392	825	37.3	78.5*	27	124*	109	150*	13.66	11.02*	94	86*
P12M	Left Parietal	408	695	38.8	66.2*	34*	94*	1*	84*	9.22*	12.81*	96	86*
P13F	Vertex	253	340	57.4	77.6	61	120	56	56	13.87	16.39	69	78
P13F	Occiput	179	301	40.3	67.4	38	114	35	39	12.51	11.41	79	82
P13F	Forehead	214	280	48.2	62.7	48	103	40	32	10.64	10.93	83	85
P13F	Right Parietal	172	211	38.6	46.9	35	66	23	4	12.77	13.11	82	91
P13F	Left Parietal	219	211	49.1	46.9	42	58	47	12	10.66	15.7	88	96
P14M	Vertex	610	1328	35.4	76.9	28	118	98	180	17.11	12.4	78	79
P14M	Occiput	650	1236	37.6	71.6	31	115	104	204	17.24	14.2	78	78
P14M	Forehead	656	1047	38	60.7	36	97	75	106	15.41	13.87	74	77
P14M	Right Parietal	538	903	31.2	52.3	21	67	72	372	14.88	14.27	92	96
P14M	Left Parietal	607	931	35.2	53.9	27	75	82	84	15.16	13.38	82	84
P15F	Vertex	564	968	39.6	67.6	33	116	54	130	13.61	12.65	84	68
P15F	Occiput	987	1490	69.4	104.8	83	210	316	358	8.59	7.98	81	87
P15F	Forehead	1168	1564	82.1	109.9	94	155	475	414	6.91	8	90	97
P15F	Right Parietal	703	1177	49.4	82.2	56	156	150	500	11.2	7.91	68	90
P15F	Left Parietal	902	1065	63.4	74.3	76	145	235	142	8.96	9.46	82	79
P17F	Occiput	949		37.6		38		257		14.2		73	
P17F	Forehead	757		85.6		100		84		8.24		62	
P17F	Vertex	1723		47.2		44		936		13.64		91	
P18M	Vertex	2243	2785	105.4	130.8	164	321	984	732	4.71	5.01	83	84
P18M	Occiput	2039	3212	95.8	150.8	133	376	908	1115	5.27	4.61	87	88
P18M	Forehead	2183	3114	102.6	146.3	148	416	1077	906	4.84	4.2	86	83
P18M	Right Parietal	2133	3035	100.2	142.5	123	312	1004	893	4.29	3.75	98	98
P18M	Left Parietal	1773	2625	83.3	123.3	88	241	763	772	5.74	5.62	98	96
P21F	Vertex	3752	5226	124.6	173.5	151	349	2296	2569	4.38	5.73	99	100
P21F	Occiput	3887	6287	129	208.7	169	500	2276	3105	4.43	6.44	95	96
P21F	Forehead	2736	3633	90.8	120.6	110	212	1301	1034	5.64	5.73	95	99
P21F	Right Parietal	2601	3340	86.4	110.9	84	196	1290	1072	5.94	6.72	100	100
P21F	Left Parietal	3294	4192	109.4	139.2	129	273	1747	1820	5.84	5.6	99	100

3.1. Injuries caused by “Non-destructive” drops

The 5-month-old (P12M), the 11-month-old (P15F) and the 22-month-old (P17F) sustained linear or diastatic fractures (Table 4). The 5-month-old's fracture was identified by abrupt slope changes in the force histories and was confirmed during post-test dissection. The 11-months-old's fracture was found by post-drop palpation and was later confirmed via post-test dissection. The 22-month-old's fracture was audible and was confirmed via CT scan.

No scalp lacerations occurred in any of the drops. The 5-month-old sustained a 4 cm stable linear right parietal bone fracture during the parietal impact that extended from the coronal suture to the ossification center in the middle of the right parietal bone. The fracture followed the direction of the bone fiber alignment. The 11-month-old sustained a stable diastatic linear fracture of the right coronal suture during the 30 cm right parietal impact. The fracture had very little displacement and followed the right coronal suture. The 22-month-old sustained a stable diastatic lin-

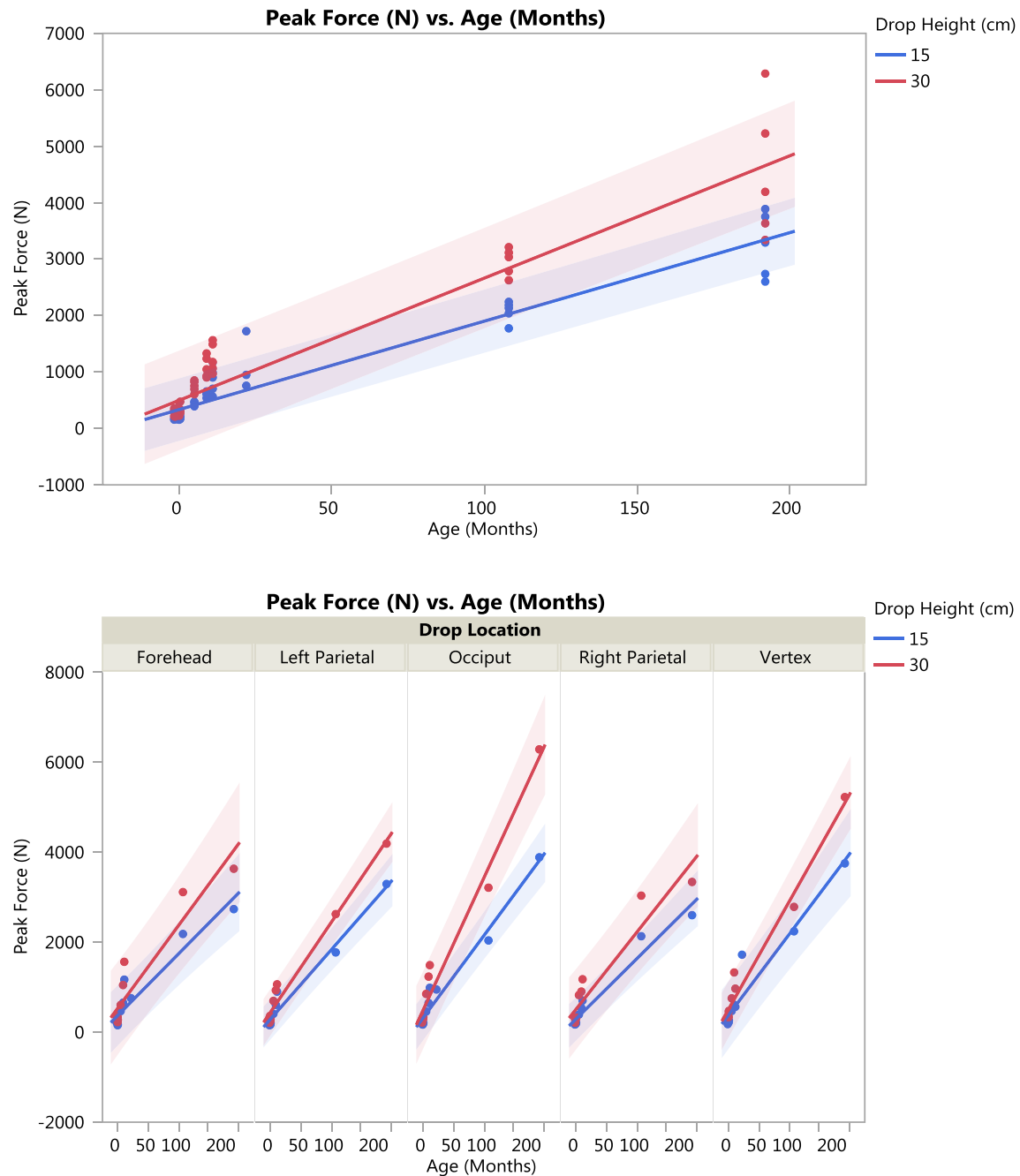


Fig. 4. (Top) The peak head force as a function of age for both 15 and 30 cm drops. For this figure, standard linear models (which do not account for the repeated nature of the testing) with prediction confidence intervals are shown for both drop heights. This was done to help the reader better visualize trends in the data since the regression models in Table 3 are multi-dimensional. Both age and drop height significantly predicted the peak force. (Bottom) Although location was not a significant predictor of peak force, the data is parsed for all five impact points for illustrative purposes.

ear fracture of the left coronal suture during the 15 cm vertex impact. A CT scan of the fracture showed that it extended across the entire length of the left coronal suture. Peak forces sustained for the three heads ranged from 392 N to 1174 N and HIC values ranged from 27 to 156 (Table 2).

4. Discussion

This study investigated the impact properties of the pediatric head. Heads were dropped onto a rigid plate and the resulting force histories were analyzed. The peak acceleration, HIC, impact stiffness and pulse duration were used to examine the effects of drop height, impact location and age.

Previous studies have conducted impact tests with the head attached to the neck in which an impactor strikes the head of a whole cadaver, as well as drop tests in which a complete cadaver or a head and neck system are dropped together (Hodgson, 1967; Hodgson and Thomas, 1971b; Nightingale, 1993). However, the current study has an isolated head in free fall, which ensures the head is evaluated without the coupling effects of the neck (Yoganandan et al., 2004). The one-dimensional motion onto a rigid surface is easy to model and is the current certification test for the Hybrid III and child ATDs (Coats et al., 2007; Foster et al., 1977; Zhang et al., 2001). However, one potential concern in conducting these tests is that air voids in the skull can allow secondary impacts of the brain with the inside of the skull to occur, which

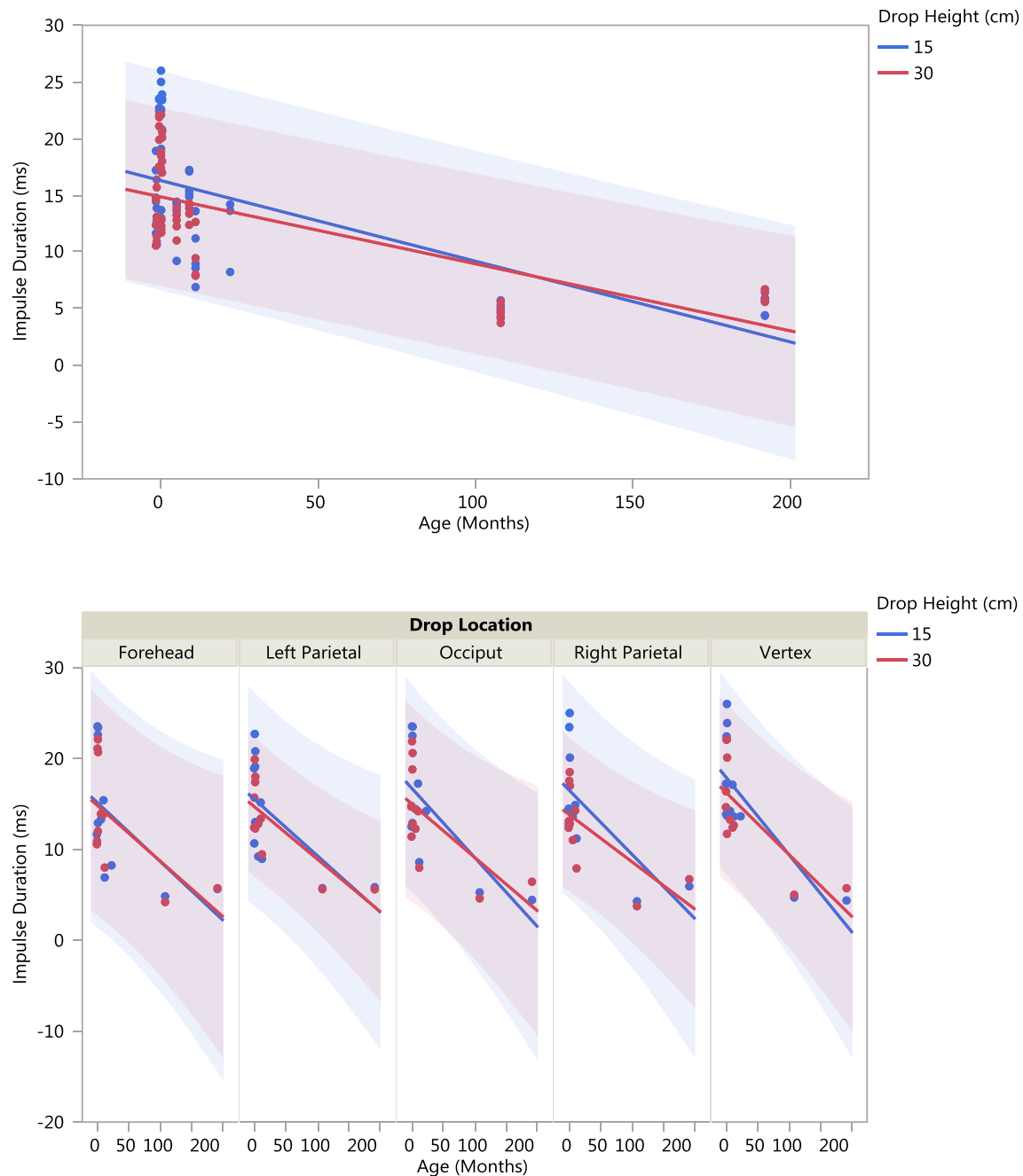


Fig. 5. The head impulse duration as a function of age for both 15 and 30 cm drops. Age, drop height and impact location were all significant predictors of impulse duration.

would be seen in the data. This did not occur in this dataset since the heads were refilled using saline to remove any air voids, forcing the brain and cerebrospinal fluid to be in contact with the inner table of the skull during impact (Prange et al., 2004).

There are limitations to this study. The first limitation is the small number of available pediatric heads, which is due to the relative rarity of pediatric deaths in the United States and the paucity of pediatric tissue donations. In addition, our sample has no data between 23-months-old and 8-years-old. The second limitation was that the heads were dropped with no mandible attached. This prevented any investigation into the head impact being coupled with the jaw. The third limitation is the boundary conditions at the foramen magnum. The head was sealed at the foramen magnum with rigid PMMA, which provided a different boundary condi-

tion than that provided by a spinal cord and cerebrospinal fluid. Fourth, the kinematics of lateral impacts are different from the kinematics of midsagittal plane impacts. Ideally, more instrumentation should be used to capture the rotation during the impact and this was not done for this study (Yoganandan et al., 2004; Zhang et al., 2009). Fifth, this analysis was conducted by examining one-dimensional motion.

4.1. Effect of age

Age was shown to have the most dominant effect on the mechanical properties of the head; age affected all of the head impact properties tested. The acceleration, HIC and dynamic stiffness all increased with increasing age, while the pulse duration

decreased with increasing age. This is consistent with our understanding of human mechanical changes with head development. Specifically, the head becomes stiffer with age as was shown in previous quasi-static head compression testing. The skull bones grow from approximately 1 mm in thickness at birth to 5–10 mm in the adult (Adeloye et al., 1975; Peterson and Dechow, 2003). The cranial bones also transform from a one layer cortical structure to a three layer structure with two cortical layers and one trabecular layer (Adeloye et al., 1975; Agur and Lee, 1991). The added thickness and the two outer layers create a stiffer structure (Margulies and Thibault, 2000; McElhaney, 1976; McElhaney et al., 1972). The mechanical characteristics of the sutures and fontanelles also change as the head develops. The sutures change from being soft and flexible to being rigidly connected. The sutures continue to stiffen as they become more interdigitated – to the point

that some have speculated that the interdigitated suture may be stiffer than bone (Cohen, 2000; Jaslow and Biewener, 1995). The fontanelle changes from being the predominant soft tissue of the skull at birth to being totally absent by the age of 2-years-old. Like the growing bone, the changes of the most compliant portion of the skull to a rigid structure will make the head stiffer. If the head is stiffer, the HIC and the peak average acceleration will increase while the contact time will decrease.

4.2. Effect of drop height

Higher drop heights caused a significantly increase in acceleration and HIC while causing a significant decrease in the pulse duration. There are two reasons for this. The first reason is that the added energy of the impact causes more compressive deformation

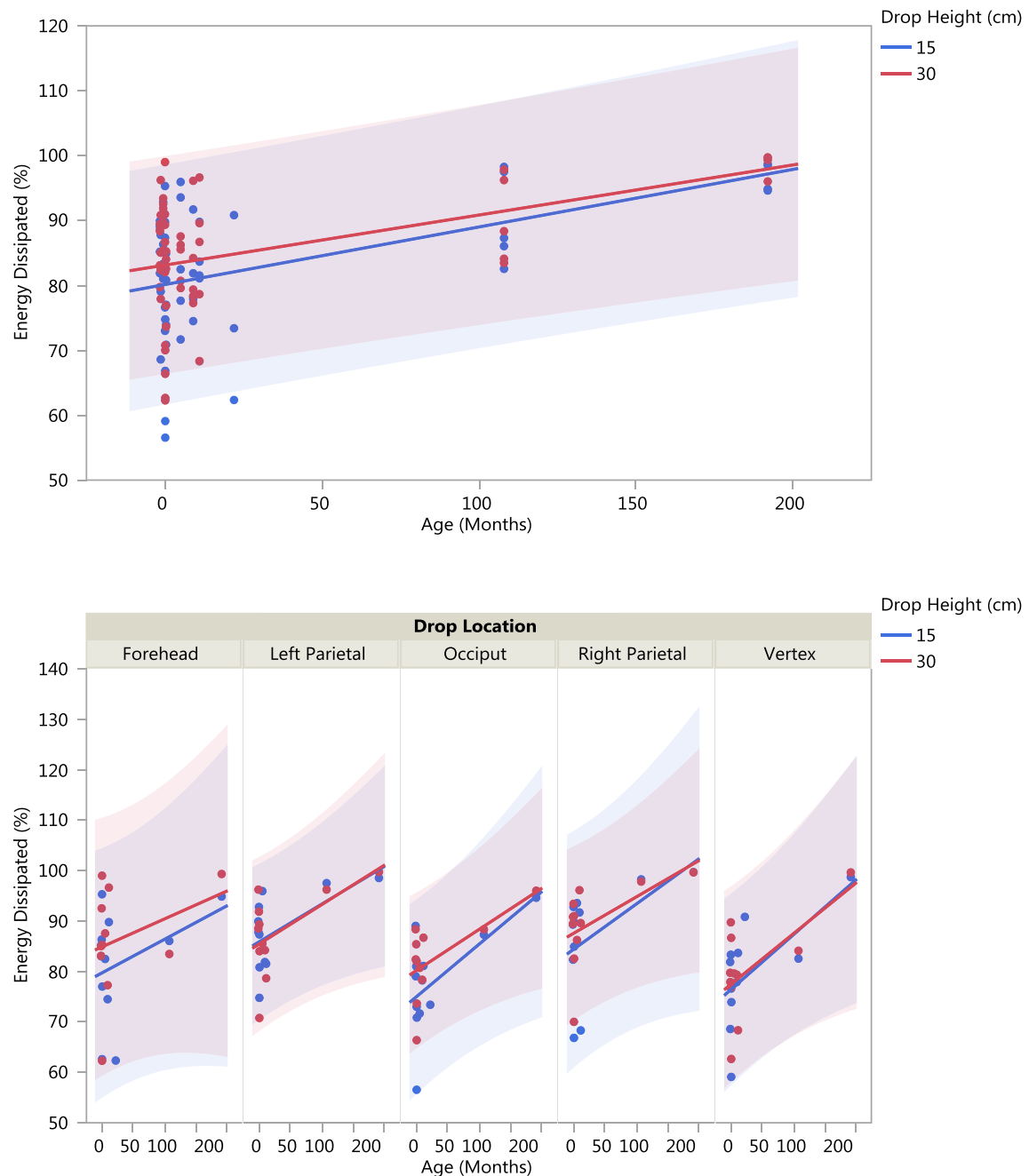
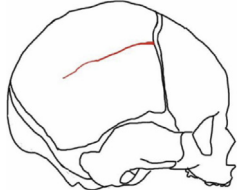

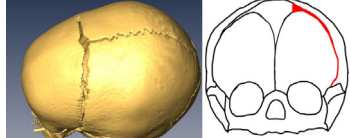


Fig. 6. The energy dissipated as a function of age for all drop heights and locations. Age was the only significant predictor of energy dissipation.

Table 3
Regression parameters for the most parsimonious model.

Dependent Variable	Term	Estimate	Standard Error	t Ratio	Prob > t	95% Lower	95% Upper
Peak Force (N)	Age (Months)	18.6	1.2	15.8200	<0.0001	15.95	21.32
	Drop Height (cm)	23.4	4.5	5.1700	<0.0001	14.44	32.40
Duration (ms)	Intercept	17.24	1.46	11.790	<0.0001	14.07	20.41
	Age (Months)	-0.06	0.02	-3.010	0.0132	-0.11	-0.02
Energy Dissipated (%)	Drop Height (cm)	-0.08	0.02	-3.740	0.0003	-0.12	-0.04
	Intercept	77.97	2.58	30.19	<0.0001	72.63	83.31
	Age (Months)	0.08	0.03	2.58	0.0279	0.01	0.16
	Drop Height (cm)	0.16	0.07	2.24	0.0274	0.02	0.29
	Drop Location [Left Parietal]	3.69	1.05	3.52	0.0007	1.61	5.78
	Drop Location [Occiput]	-3.80	1.03	-3.7	0.0004	-5.85	-1.76
	Drop Location [Right Parietal]	4.16	1.05	3.97	0.0001	2.08	6.24
Acceleration (Gs)	Intercept	12.60	5.40	2.33	0.0251	1.67	23.53
	Age (Months)	0.45	0.06	7.59	<0.0001	0.32	0.58
	Drop Height (cm)	1.82	0.17	10.45	<0.0001	1.47	2.16
	Drop Location [Right Parietal]	-5.35	2.62	-2.04	0.0438	-10.54	-0.15
HIC	Intercept	-59.43	16.05	-3.70	0.0005	-91.66	-27.19
	Age (Months)	0.95	0.16	6.00	0.0001	0.60	1.30
Stiffness (N/mm)	Drop Height (cm)	5.76	0.56	10.27	<0.0001	4.65	6.87
	Intercept	55.19	20.80	2.65	0.0263	8.13	102.25
	Age (Months)	9.07	0.31	28.81	<0.0001	8.35	9.78

Table 4
Fractures that occurred during the head drops.

Specimen	Age (mo.)	Height and Location	HIC	Peak Acceleration (g)	Peak Force (N)	Fracture
P12M	5	15 cm Right Parietal	27	37.3	392	
P15F	11	30 cm Right Parietal	156	82.2	1174	
P17F	22	15 cm Vertex	44	47.2	949	

of the head during impact. As the deformation increased the head rebounded to produce higher HIC and acceleration. The second reason is that the head shows viscoelastic behavior, especially at earlier ages. This tends to increase force response for higher rate impacts.

4.3. Effect of impact location

The impact location was shown to be a significant variable for the pulse duration and acceleration. The vertex produced the highest values for acceleration, HIC and dynamic stiffness while impacts to the parietal location showed the lowest acceleration, HIC and dynamic stiffness. This has been shown in previous impact studies of adult and ATD head response (Loyd et al., 2014). Like the adult and ATD head, this difference is largely due to the differences

in head kinematics. For the vertex drops, the impact direction was in the line of action of the center of gravity of the head which caused higher accelerations, higher HIC values and lower pulse durations. For the parietal impacts, the center of gravity of the head was not aligned with the impact location, which produced lower accelerations and HIC values.

4.4. Impact stiffness vs. Quasi-static stiffness

The impact stiffness and quasi-static stiffness of the heads were found to be significantly different: the dynamic stiffness was found to be more than five times greater than the quasi-static stiffness (Fig. 7). These facts indicate that the head response could be rate-dependent or that the mechanics of head impact are governed by the local contact stiffness of the head, or both.

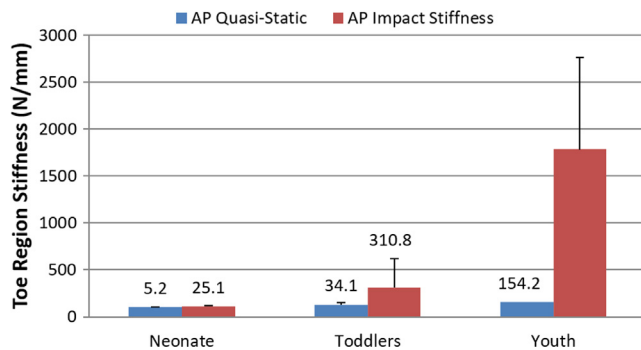


Fig. 7. The toe region stiffness (1.25% to 2.5% of the max head length) quasi-static stiffness and impact stiffness of the human head versus age. The AP dynamic stiffness were taken from the average of the 30 cm occipital and forehead impact stiffnesses. Neonates were less than 1-month-old. Toddler was the 5, 9, 11 and 22-month-old. The youth were the 9 and 16-year-old.

4.5. Fractures

Three of the four heads between 5-months-old and 22-months-old (infants) sustained fractures in the 15 cm or 30 cm drops. However, none of the neonatal heads and none of the heads 9-years-old and older sustained fractures in the tests. This result suggests that there is a period in the first few years of life in which the skull is susceptible to fracture at drop heights of less than 30 cm, a finding that has not been previously reported. This age-dependent injury trend is likely the result of normal skull development. In neonates, the skull is relatively compliant because the sutures have not yet begun to fuse (Cohen, 2000). Consequently, neonatal skulls are able to deform without fracture when dropped from low heights, making them less susceptible to fracture than slightly older children. However, the deformation experienced by these neonatal skulls during impact may result in soft tissue injuries of the sort that cannot be examined using a cadaver model.

On the other hand, the heads in the age range from 5 to 22-months-old do not share these same properties. The result suggests an age of vulnerability to impacts from small heights. Three of the four infant heads fractured during these drops; which did not occur with the neonates, 9-year-old and 16-year-old heads. At 5-months-old, the suture begins to fuse at this time so that the connections between the bone plates are rigid yet weak making the skull vulnerable to fracture, particularly diastatic fractures (Davis et al., 2012). These types of pediatric diastatic suture fractures have not been frequently documented in the literature cf. (Bilo et al., 2010). Diastatic suture fractures may be underreported because a diastatic suture fracture appears as a non-fused suture on CT scans or plain film X-rays. Mulroy et al. showed that X-ray only detected 42% of diastatic suture fractures (Mulroy et al., 2012). In addition, Davis et al. showed that fused sutures may fracture and lose all ability to resist a moment, however the two bone plates will remain attached (Davis et al., 2012).

The fracture of the 5-month-old head occurred as a linear fracture on the right parietal bone. The fracture terminated at the coronal suture and in the middle of the right parietal bone. This correlates with reports that the parietal bone is the most frequently fractured location in the child's skull (Bilo et al., 2010). Using cadaveric drops, Weber argued that the parietal bones were the most susceptible to fracture (Weber, 1987). There are two reasons for the high incidence of fracture in the parietal bone. The first is that the parietal bone has the largest surface area and is simply the most likely bone to be struck during an impact. Second, the parietal bone is the thinnest region of bone in the skull.

The fracture results for the infant are surprising because they suggest that at this age, fracture can occur at low drop heights

(<82 cm) such as those experienced from a fall from a bed, chair or couch. This is directly in agreement with Weber that the pediatric skull is susceptible to fracture at low heights (Weber, 1987).

The HIC values of 27 to 156, reported for the infant-aged drops which fractured, were less than the non-fractured impacts. This is most likely because the skull fracture absorbs strain energy, which reduces the peak acceleration as well as the impulse duration. It is unknown if a child between 5 and 22-months-old would sustain brain injury from the acceleration values reported here. It may be possible that fracture can occur without any type of brain trauma or the bone displacement due to the fracture may cause intracranial bleeding or other associated injuries.

5. Conclusions

This study provides the first collection of head impact data for pediatric heads ranging in age from neonate to 16-years-old. It provides data for five head impact locations at two different drop heights. The human heads were tested to find the effects of drop height, impact location and age upon the impact properties.

This study demonstrated that age, drop height and drop location are all important factors in the response of the human head. Age was the most dominant factor, as the stiffness of the head increased with age. This caused the head to respond with higher dynamic stiffness, acceleration and HIC values. The heads also responded with higher acceleration with increased drop height.

This study provides valuable failure data for the pediatric head which has never been previously reported. This study indicates that for falls onto a rigid surface from 30 cm, fractures rarely occur for neonates. This study also shows that for falls from this height, fracture can occur for children between the ages of 5 and 22-months-old, and that these fractures appear as linear or diastatic fractures for impacts onto a flat surface.

Declaration of Competing Interest

The authors declare that there is no conflict of interest regarding the content of this article.

Acknowledgments

The authors thank NHTSA under contract DTNH22-94-Y-07133 and the Southern Consortium for Injury Biomechanics at the University of Alabama Birmingham for providing funding for this research. We also thank the National Science Foundation for Dr. Loyd's graduate school fellowship.

References

- Adeloye, A., Kattan, K.R., Silverman, F.N., 1975. Thickness of the normal skull in the American blacks and whites. *Am. J. Phys. Anthropol.* 43, 23–30.
- Agur, A.M.R., Lee, M.J., 1991. *Grant's Atlas of Anatomy*. Williams & Wilkins, Baltimore.
- Billmire, M., Myers, P., 1985. Serious head injury in infants: accident or abuse? *Pediatrics* 75, 340–342.
- Bilo, R.A.C., Robben, S.G.F., Rijn, R.R.V., 2010. *Head, Forensic Aspects of Paediatric Fractures: Differentiating Accidental Trauma from Child Abuse*. Springer, London, pp. 15–48.
- Coats, B., Margulies, S.S., 2006. Material properties of human infant skull and suture at high rates. *J. Neurotrauma* 23, 1222–1232.
- Coats, B., Margulies, S.S., Ji, S., 2007. Parametric study of head impact in the infant. *Stapp Car Crash J.* 51, 1–15.
- Cohen, M.M., 2000. Suture biology. In: Michael Cohen, M.J., MacLean, R.E. (Eds.), *Craniosynostosis: Diagnosis, Evaluation, and Management*. second ed. Oxford University Press, New York, pp. 11–22.
- Currey, J.D., Butler, G., 1975. Mechanical properties of bone tissue in children. *J. Bone Joint Surg.* 57-A, 810–814.
- Davis, M.T., Loyd, A.M., Shen, H.-y.H., Mulroy, M.H., Nightingale, R., Myers, B., Bass, C.D., 2012. The mechanical and morphological properties of 6-year-old cranial bone. *J. Biomech.* 45, 2493–2498.

- Faul, M., Xu, L., Wald, M.M., Coronada, V.G., 2010. Traumatic brain injury in the United States: emergency department visits, hospitalizations and deaths 2002–2006. In: Control, N.C.f.i.P.a. (Ed.), National Center for Injury Prevention and Control, Atlanta, GA, p. 71.
- Foster, J., Kortge, J., Wolanin, M., 1977. A biomechanically based crash test dummy. In: Stapp Car Crash, J., Warrendale, P.A. (Eds.).
- Gurdjian, E.S., Webster, J.E., Lissner, H.R., 1950. The mechanism of skull fracture. *Radiology* 54, 313–339.
- Hobbs, C., 1984. Skull fracture and diagnosis of abuse. *BMJ*, 245–252.
- Hodgson, V.R., 1967. Tolerance of the facial bones to impact. *Am. J. Anat.* 120, 113–122.
- Hodgson, V.R., Thomas, L.M., 1971a. Breaking strength of the human skull versus impact surface curvature. In: Administration, N.H.T.S. (Ed.). National Highway Traffic Safety Administration.
- Hodgson, V.R., Thomas, L.M., 1971b. Comparison of head acceleration injury indices in cadaver skull fracture. *Stapp Car Crash J.* 15, 190–206.
- Ilie, G., Adlaf, E.M., Mann, R.E., Boak, A., Hamilton, H., Asbridge, M., Colantonio, A., Turner, N.E., Rehm, J., Cusimano, M.D., 2014. The moderating effects of sex and age on the association between traumatic brain injury and harmful psychological correlates among adolescents. *PLoS One* 9, 1–14.
- Jaslow, C.R., Biewener, A., 1995. Strain Patterns in the horncores, cranial bones and sutures of goats (*Capra hircus*) during impact loading. *J. Zool.* 235, 193–210.
- Kleinberger, M., Sun, E., Eppinger, R., Kuppa, S., Saul, R., 1998. Head Injury Criteria, Development of Improved Injury Criteria for the Assessment of Advanced Automotive Restraint Systems. NHTSA, Washington D.C. pp. 12–17.
- Klinich, K.D., Hulbert, G.M., Schneider, L.W., 2002. Estimating infant head injury criteria and impact response using crash reconstruction and finite element modeling. *Stapp Car Crash J.* 46, 165–194.
- Leventhal, J.M., Thomas, S.A., Rosenfield, N.S., Markowitz, R.I., 1993. Fractures in young children: distinguishing child abuse from unintentional injuries. *Am. J. Dis. Child.* 147, 87–92.
- Loyd, A., Nightingale, R., Luck, J., Song, Y., Fronheiser, L., Cutcliffe, H., Myers, B., Bass, D., 2015. The compressive stiffness of human pediatric heads. *J. Biomech.* 48, 3766–3775.
- Loyd, A.M., Nightingale, R.W., Song, Y., Luck, J.F., Cutcliffe, H., Myers, B.S., Bass, C.D., 2014. The response of the adult and ATD heads to impacts onto a rigid surface. *Accid. Anal. Prev.* 72, 219–229.
- Luck, J.F., Nightingale, R.W., Loyd, A.M., Prange, M.T., Dibb, A.T., Song, Y., Fronheiser, L., Myers, B.S., 2008. Tensile mechanical properties of the perinatal and pediatric PMHS osteoligamentous cervical spine. *Stapp Car Crash J.* 52, 107–134.
- Luck, J.F., Nightingale, R.W., Song, Y., Kait, J.R., Loyd, A.M., Myers, B.S., Cameron, R., Bass, C.R., 2013a. Tensile failure properties of the perinatal, neonatal, and pediatric cadaveric cervical spine. *Spine* 38 (1), E1–E12.
- Luck, J.F., Nightingale, R.W., Bass, C.R., 2013b. Compressive mechanical properties of the perinatal, neonatal and pediatric cervical spine. In: Proceedings of the International Conference on the Biomechanics of Injury; Gothenburg, pp. 655–662.
- Manzanares, M., Goret-Nicaise, D.A., 1988. Metopic sutural closure in the human skull. *J. Anat.* 161, 203–215.
- Margulies, S.S., Thibault, K.L., 2000. Infant skull and suture properties: measurements and implications for mechanisms of pediatric brain injury. *J. Biomech. Eng.* 122, 364–371.
- McElhaney, J., 1976. Biomechanical aspects of head injury. *Mekhanika Polimerov* 3, 465–477.
- McElhaney, J., Stalnaker, R., Roberts, V.L., 1972. Biomechanical aspects of head injury. In: King, W., Mertz, H.J. (Eds.), Human Impact Tolerance. Plenum Press, New York, pp. 85–112.
- McKinlay, A., Grace, R., Horwood, L., Fergusson, D., Ridder, E., MacFarlane, M., 2008. Prevalence of Traumatic brain injury among children, adolescents and young adults: prospective evidence from a birth cohort. *Brain Inj.* 22, 175–181.
- Melvin, J.W., 1995. Injury Assessment Reference Values for the CRABI 6-Month Infant Dummy in a Rear-Facing Infant Restraint with Airbag Deployment. SAE Technical Paper Series.
- Mertz, H., Jarrett, K., Moss, S., Salloum, M., Zhao, Y., 2001. The hybrid III 10-year-old Dummy. *Stapp Car Crash J.* 45, 319–328.
- Mulroy, M.H., Loyd, A.M., Frush, D.P., Verla, T.G., Bass, C.D., Myers, B.S., 2012. Evaluation of pediatric skull fracture imaging techniques. *Forensic Sci. Int.* 214, 167–172.
- Nightingale, R.W., 1993. The Dynamics of Head and Cervical Spine Impact. Dissertation. Duke University, Durham.
- Peterson, J., Dechow, P.C., 2003. Material properties of the human cranial vault and Zygoma. *Anatom. Record Part A: Discov. Mol. Cell. Evolut. Biol.* 274A, 785–797.
- Prange, M., Luck, J., Dibb, A., Ee, C.V., Nightingale, R., Myers, B., 2004. Mechanical properties and anthropometry of the human infant head. *Stapp Car Crash J.* 48, 279–299.
- SAEJ222-1, 1995. SAE J211/1- Instrumentation for impact test part 1: Electronic Instrumentation Society, Society of Automotive Engineers.
- Van-Ee, C., Moroski-Browne, B., Raymond, D., Thibault, K., Hardy, W., Plunkett, J., 2009. Evaluation and refinement of the CRABI-6 anthropomorphic test device injury criteria for skull fracture. ASME 2009 International Mechanical Engineering Congress & Exposition. Lake Buena Vista, Florida.
- van-Ratingen, M.R., Twisk, D., Schrooten, M., Beusenbergh, M.C., Barnes, A., Platten, G., 1997. Biomechanically Based Design and Performance Targets for a 3-Year Old Child Crash Dummy for Frontal and Side Impact. Society of Automotive Engineers International.
- Walker, L., Harris, E., Pontius, U., 1973. Mass, volume, center of mass, and mass moment of inertia of head and head and neck of human body. *Stapp Car Crash Conference 17th*, 525–537.
- Weber, W., 1984. Experimentelle Untersuchungen zu Schädelbruchverletzungen des Säuglings (Experimental Study of Skull Fractures in Infants). *Zeitschrift für Rechtsmedizin* 92, 87–94.
- Weber, W., 1985. Zur biomechanischen Fragilität des Säuglingsschädels (Biomechanical Fragility of the infant skull). *Z. Rechtsmed.* 94, 93–101.
- Weber, W., 1987. Prädispositionsstellen infantiler Kalottenfrakturen nach stumpfer Gewalt (Preferred Site of Skull Fractures in Infants). *Z. Rechtsmed.* 98, 81–93.
- Yoganandan, N., Zhang, J., Pintar, F.A., 2004. Force and acceleration corridors from lateral head impacts. *Traffic Inj. Prevent.* 5, 368–373.
- Zhang, J., Yoganandan, N., Pintar, F.A., 2009. Dynamic biomechanics of the human head in lateral impacts. *Ann. Adv. Automotive Med.* 53, 249–256.
- Zhang, L., Yang, K.H., King, A.I., 2001. Biomechanics of Neurotrauma. *Neurol. Res.* 23, 144–156.